

Broad Band Focusing and Demultiplexing of In-Plane Propagating Surface Plasmons

Lin Li,[†] Tao Li,^{*,†} Shuming Wang,[†] Shining Zhu,[†] and Xiang Zhang[‡]

[†]National Laboratory of Solid State Microstructures, School of Physics, College of Engineering and Applied Sciences, Nanjing University, Nanjing 210093, China

[‡]Nanoscale Science and Engineering Center, 5130 Etcheverry Hall, University of California, Berkeley, California 94720-1740, United States

S Supporting Information

ABSTRACT:



On the basis of a novel phase modulation method by in-plane diffraction processes, a well-designed nanoarray on metal surface is proposed to realize a broad band focusing (bandwidth ~ 100 nm) and a demultiplexing element (resolution ~ 12 nm) of surface plasmon polariton (SPP) waves. Moreover, sublattice arrays are developed to achieve an improved demultiplexer and confocal SPP beams. The proposed scheme with implemented functionalities is designed totally in planar dimension, which is free of the SPP coupling process and indicates more practical application in photonic integrations.

KEYWORDS: Surface plasmon polariton, broad band focusing, wavelength demultiplexer, in-plane photonic integration

As a promising carrier for the new generation information technology, surface plasmon polaritons (SPPs) have generated great research enthusiasm.¹ Owing to the unique two-dimensional (2D) confinement of electromagnetic (EM) field at the metal surface, SPPs provide great possibilities to route the EM energy at subwavelength scale in a planar dimension.^{2–5} Some plasmonic devices have been successfully realized, such as SPP launchers and focusing,^{6–9} waveguides,^{10,11} Bragg mirrors,¹² and so on. Among them, plasmonic demultiplexer is of extreme importance for the wavelength division multiplexing and spectral imaging.¹³ To date, most of these devices are based on periodic structural designs and implement their functions via Bragg condition, which inevitably limit their facilities to a certain particular wavelength. More recently, some impressive approaches based on nonperiodic structures have been reported on the SPP focusing¹⁴ as well as the wavelength demultiplexing.^{15,16} However, these approaches severely depend on the coupling processes with the whole structure covered by out-plane incident light, which goes against a full manipulation of in-plane SPP and would be harmful to practical photonic integrations.

In this work, we experimentally demonstrate a broad band SPP focusing directly from a propagating SPP wave by a newly developed phase modulation method, which is free of strict Bragg

diffraction condition.¹⁷ The SPP waves of different wavelengths (within a wide range about 100 nm) are effectively focused to different positions, which is capable of working as a plasmonic demultiplexer in planar integrations with a relative high resolution. Moreover, sublattice designs are developed to further promote our devices, by which an improved demultiplexer and SPP confocal properties are definitely achieved. All of these proposed designs are free of the SPP coupling process, indicating more practical SPP modulations in a totally planar dimension.

First, we would demonstrate the SPP focusing property for a single wavelength. A novel nonlinear phase modulation method for propagating SPPs by diffraction from nonperiodic array was introduced,¹⁷ where the equivalent phase has an extra 2π change when the incident surface wave pass through a unit row of the nanoarray with the local lattice parameter gradually changed in the wave propagation direction (x axis). The corresponding phase evolution in the x direction (at the m th rows) with respect to every diffracted SPP wave can be written as $\phi(x) = \phi_0 + k_{\text{spp}}x - 2m\pi$ (details see ref 17 and the Supporting Information therein).

Received: July 21, 2011

Revised: September 16, 2011

Published: September 22, 2011

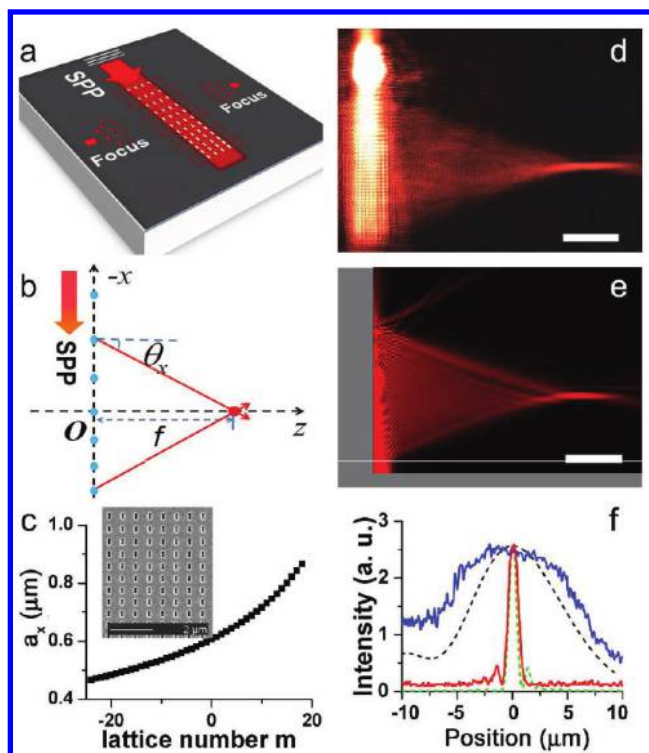


Figure 1. (a) Schematic of SPP focusing by nanoarray diffractions from an incident SPP beam. (b) Design scheme of the nonperiodic array for the SPP focus. (c) Parameters of the designed nonperiodic lattice in the x dimension for a horizontal beaming focus. Lattice sequence number is normalized to the beam center of the focusing (O point). Inset is the top-view image of the sample fabricated by FIB. (d) Experimental result of horizontal focusing detected by LRM system. (e) The corresponding theoretical result. (f) Profiles of the focal spots for experimental (solid line) and theoretical results (dash line). The blue and black curves are the longitudinal profiles (z direction), and the red and green curves are the transverse ones (x direction) (scale bar = $10 \mu\text{m}$).

Here ϕ_0 is the initial phase of the incident wave and m is the sequence number of the lattice point along the x direction. On the basis of this method, a square phase evolution used for EM wave focusing will be fulfilled. According to the equivalent phase evolution by the diffraction process above, the location of the m th diffraction unit can be deduced by solving $\phi_m(x) = \psi(x)$, and we will ultimately retrieve the arrangement of nanocave array, in which $\psi(x) = -kx^2/2f_0$ is the square phase evolution with focal length of f_0 for a corresponding wave vector of k .

Panels a and b of Figure 1 schematically show our design, where an in-plane SPP wave launched by a focused laser with a grating coupler directly incidents into a nonperiodic nanocave array. By appropriately arranging the nanoarray, diffracted SPP waves are focused to two spots on both sides. In experiments, the nanoarray was fabricated by the focused ion beam (Strata FIB 201, FEI Company) on a 60 nm thick silver film that was sputtered on a SiO_2 substrate (see the top view image shown in the inset of Figure 1c). An x -directional SPP wave was launched from a focused laser by the coupling of a groove grating with the period of 610 nm and depth of 20 nm, which consequently incidents into the nanoarray. The SPP propagation and diffractions were detected by a home-built leakage radiation microscope (LRM) system^{18,19} with an oil-immersion lens ($160\times$, NA = 1.4). The designed parameters of graded local lattice parameter a_x in the

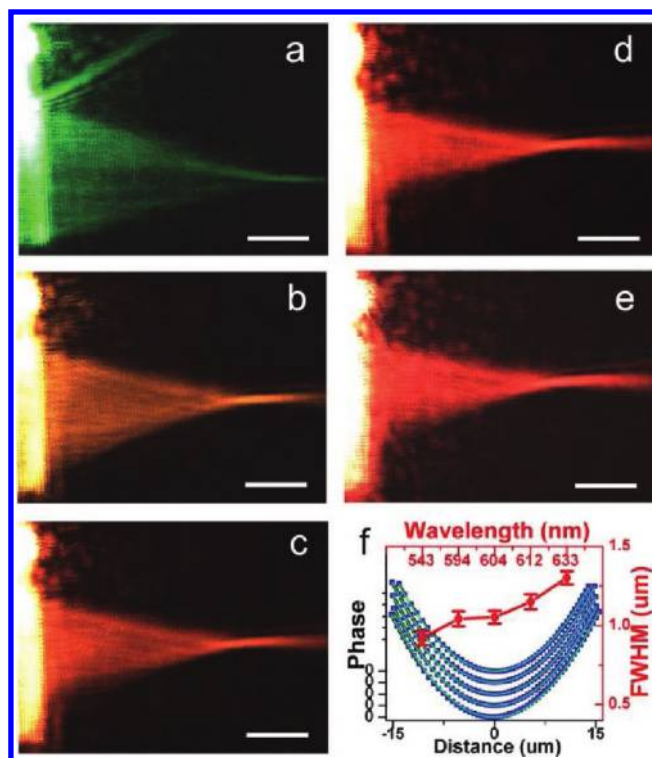


Figure 2. Broad band SPP focusing results. (a–e) Experimental results detected by the LRM system corresponding to lasers with λ_0 of 543, 594, 604, 612, and 633 nm, where the scale bar = $10 \mu\text{m}$. (f) fwhm's measured in a–e in red circle symbols. The blue square symbols are the deduced phase from the units of the array for $\lambda_0 = 543, 594, 604, 612,$ and 633 nm corresponding from bottom to top, and the green curves are the analytical square phase evolution for focus.

x direction (determined by the mean value of two distances before and after the lattice of x) are shown in Figure 1c and the lateral period in the z direction is $p_z = 640$ nm. All nanocave units are rectangular ($120 \text{ nm} \times 240 \text{ nm}$, the long side along the x direction) with a depth of about 20 nm. Figure 1d is a typical SPP focus result with horizontal focal length of $f = 40 \mu\text{m}$ for an SPP wavelength of $\lambda = 610$ nm (from $\lambda_0 = 633$ nm a He–Ne laser). To compare with the experimental result, we performed a theoretical calculation based on the Huygens–Fresnel principle, in which all nanocaves in the array are considered as subsources that radiate cylindrical SPP waves.^{15,20} The calculated field intensity distribution is shown in Figure 1e, which shows good agreement with the experimental one. To get a clear evaluation of the focusing property, the profiles of the focal spots are shown in Figure 1f, whose full widths at half-maxima (fwhm) of experimental result are about 12.2 and $0.93 \mu\text{m}$ in longitudinal (z) and transverse (x) dimensions, respectively, agreeing well with the calculated value of 9.35 and $0.82 \mu\text{m}$ accordingly. It is worth mentioning that the SPP intensity at the foci (about $60 \mu\text{m}$ away from the SPP source—the grating coupler) is as strong as that of only $20 \mu\text{m}$ distance away from the source due to a focusing effect, which indicates great usage in routing the SPP energy to overcome the large losses.

It is interesting to notice that the designed lattice parameters have almost a linear increment in the x direction (defined as Δx), which indicates the applicability for other wavelength SPPs and implies the possibility of a broad band focusing. The assumption is proved by our experiments. The structure is designed for a

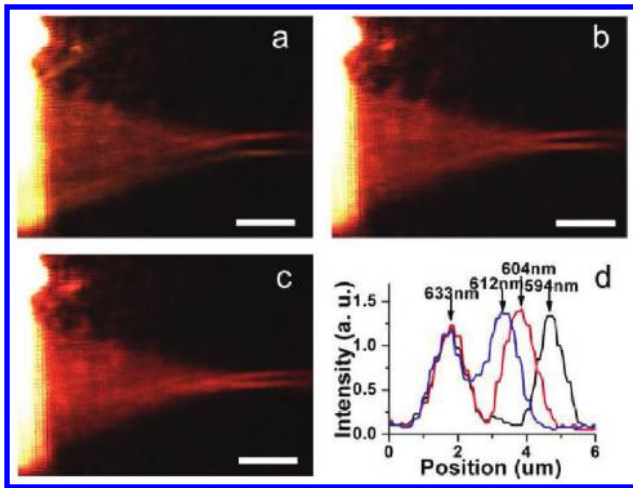


Figure 3. SPP demultiplexing for dual-wavelength beams. LRM detected focusing SPP trajectories of free-spaces wavelength $\lambda_1 = 633$ nm and λ_2 of (a) 594 nm, (b) 604 nm, and (c) 612 nm, scale bar = 10 μm . (d) The transverse focus profiles of the focal spots.

horizontal focusing with $f = 40 \mu\text{m}$ for the SPP of $\lambda = 560$ nm ($\lambda_0 = 580$ nm) and the period in the z direction is $p_z = 560$ nm. The experimental results are shown in panels a–e of Figure 2, corresponding for the incident five-color He–Ne laser beams of $\lambda_0 = 543, 594, 604, 612,$ and 633 nm, which reveals evident focusing property for these five-color SPP beams over a wide wavelength range of about 100 nm. The transverse fwhm's of these foci are from 0.9 to 1.3 μm as shown in Figure 2f (circular symbol with error bars). By carefully clarifying the optical axis of focusing beam at different wavelengths, we also deduce the phase evolutions as shown in Figure 2f (square symbols), which match the square type curves considerably well, indicating all SPPs in different wavelengths can be well focused. Nevertheless, the phase deviation from the square-type tends to increase when the wavelength is far from the designed one. A better focus can be fulfilled with a careful trade-off between the required wavelength and a desired bandwidth. Here, our experiments have exhibited the focusing results, which are good enough for a bandwidth of at least about 100 nm in the visible region.

To demonstrate the demultiplexing for multiwavelength SPPs more precisely, another He–Ne laser (633 nm) is employed as a reference together with the five-color laser to produce a dual-wavelength SPPs source. Panels a–c of Figure 3 are the experimental results corresponding to the incident laser beams of 633 nm together with 594, 604, and 612 nm in turn. The LRM detected intensity profiles at the focal spots are shown in Figure 3d. From these data, we can retrieve a relation between the focal distance (d) and the wavelength differences ($\Delta\lambda$), and therefore obtain a function of $\Delta\lambda(d)$. At the same time, an average fwhm_a of the profile peaks (corresponding to the focal spots) can be obtained, which indeed determines the resolution of SPP demultiplexer as

$$R = \Delta\lambda(d = \text{fwhm}_a) \quad (1)$$

Strictly, the fwhm is also a function of designed SPP wavelength, using an average value to determine the resolution is not a very accurate one. However, fwhm's of focal spots of the nearby wavelengths change very little that can be regarded as almost the same in retrieving the resolution (R). Therefore, the definition of

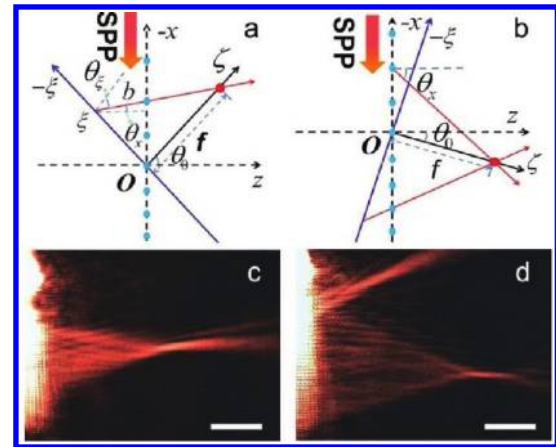


Figure 4. Schematic designs for focusing with up-inclined optical axis (a) and the down-inclined one (b). (c, d) Corresponding experimental results of (a) and (b), respectively. The period in z direction is 630 nm for (c) and 670 nm for (d) (scale bar = 10 μm).

eq 1 is suitable and convenient. As for our results of the concerned SPP wavelength of around 600 nm, the retrieved resolution R is 12 nm. A higher resolution is reasonably expected by more careful modulation of the focusing parameters (e.g., larger NA, larger focal lengths, etc.).

Furthermore, with the help of this phase modulation method, SPP focus with any arbitrary optical axis with respect to the SPPs propagating direction can be realized. The mechanisms are schematically shown in panels a and b of Figure 4, corresponding to the up-inclined and down-inclined focuses, respectively. The phase information of the nonperiodic nanoarray can be deduced with respect to a new coordinate ξ , which is perpendicular to the expected optical axis (angle of θ_0 with respect to the z direction). According to the principle of geometric optics, we have

$$\psi(\xi) = \psi(x) - k_{\text{spp}}b \quad (2)$$

Here, $\psi(\xi)$ is the desired phase for the focusing design

$$b = -\frac{x \tan(\theta_0)}{\cos(\theta_x) + \tan(\theta_0) \sin(\theta_x)} \quad (3a)$$

$$\xi = \frac{x}{\cos(\theta_0)(1 + \tan(\theta_x) \tan(\theta_0))} \quad (3b)$$

and $\sin(\theta_0) = (\lambda_{\text{spp}} - a_0)/a_0$ and $\sin(\theta_x) = (\lambda_{\text{spp}} - a_x)/a_x$. The arrangement of nanoarray can be acquired simply as above method by solving $\phi_m(x) = \psi(x)$, in which $\psi(x)$ is derived from eq 2.¹⁷ Panels c and d of Figure 4 are the experimental results of the SPP focus with $f = 30$ and $40 \mu\text{m}$ and angle of $\theta_0 = 10^\circ$ and -5° , respectively, which well reproduce our designs.

Illuminated by above designs and results, a more flexible wavelength demultiplexer with improved resolution is proposed. The device is based on two sets of sublattice A (blue) and B (green), which are specially designed corresponding to two SPP beams of wavelengths of 610 and 570 nm, respectively, as schematically shown in Figure 5a. According to the introduced phase modulation method, the focusing trajectories will be maintained if the longitudinal lattice parameters (a_x) are unchanged, while the focusing intensity will be modified with different lateral lattice constant (p_z). Figure 5b shows the different focal intensities with respect to different p_z for both waves (two blue curves result from

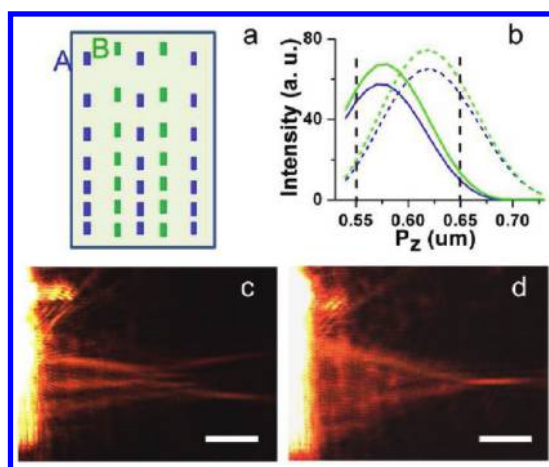


Figure 5. (a) Schematic for diplexer design with a dual sublattice (A designed for SPP wavelength of 610 nm and B for 570 nm). (b) Calculated focus intensities with respect to different lattice of p_z , which are designed corresponding to two different SPP waves (blue curves to sublattice A and green ones to B). The solid and dotted curves are the calculated focusing results of SPPs with $\lambda = 570$ and 610 nm, respectively, for both two sublattices. (c) Experimental result for improved wavelength demultiplexer for two SPP beams ($\lambda = 570$ and 610 nm) designed by the dual sublattice design (upper focus for sublattice A and lower one for B), where lattice periods p_z are indicated by two vertical dashed lines (at about 650 and 550 nm for sublattice A and B, respectively) in (b). (d) Experimental confocal result for the two SPP beams as in (c) by nanoarray with periods p_z the as same as in (c) while different a_x , where scale bars = 10 μm . All lattice data of a_x are provided in the Supporting Information.

the sublattice A with respect to SPPs of $\lambda = 570$ nm (solid) and 610 nm (dotted), and two green curves to sublattice B correspondingly). Here we select $p_z = 0.65 \mu\text{m}$ for sublattice A and $p_z = 0.55 \mu\text{m}$ for B, which are chosen with strong intensity contrast for different wavelengths as shown in Figure 5b. With this design, an improved demultiplexer is shown in Figure 5c, where the focal spots for SPP beams of $\lambda = 570$ nm and 610 nm are evidently separated to a larger distance ($\sim 7 \mu\text{m}$ much larger than 3 μm in Figure 3d) as expected. Moreover, this sublattice structure even can be modulated to achieve the confocal property for the dual beams as shown in Figure 5d, where both beams are focalized to the same spot with a same foci of $f = 40 \mu\text{m}$ (for design details see the Supporting Information). So far, it is well demonstrated that our sublattice method is so flexible that it can modulate the focusing and demultiplexing properties almost at will. Nevertheless, one point should be mentioned that in this kind of sublattice design more noises are usually introduced than the uniform ones in Figures 1, 2, and 3. In this regard, the uniform and sublattice designs can be selectively adopted for some specific purposes.

In conclusion, we proposed and demonstrated a broad band focusing and demultiplexing of thoroughly in-plane propagating SPP waves by well-designed nonperiodic nanocave arrays, in which a bandwidth of at least 100 nm of focusing and a resolution as high as 12 nm for wavelength demultiplexer were obtained. Moreover, the focusing properties, including focusing direction and length, can be designed by careful phase modulations, based on which a sublattice design is proposed to further improve the demultiplexing property and even to achieve the confocal SPP dual beams. All experimental results as well as the design method do offer us a new way to route the SPP beams totally in a planar

platform without relying on the coupling process, which is much closer to the practical vision for the future in-plane photonic integrations.

■ ASSOCIATED CONTENT

S Supporting Information. All nonperiodic nanoarray lattice data in the x direction (a_x) are provided in Figure S1, the corresponding period in the z direction (p_z) is given in the figure caption as well, and supplementary results for SPP confocal property are supplied for two different wavelengths (red and yellow lasers) in Figure S2. This material is available free of charge via the Internet at <http://pubs.acs.org>

■ AUTHOR INFORMATION

Corresponding Author

*E-mail: taoli@nju.edu.cn. URL: <http://dsl.nju.edu.cn/litao>.

■ ACKNOWLEDGMENT

This work is supported by the State Key Program for Basic Research of China (Nos. 2012CB921501, 2010CB630703, 2009CB030501, and 2011CBA00200) and the National Natural Science Foundation of China (Nos. 11174136, 10974090, 60990320, and 11021403).

■ REFERENCES

- (1) Ozbay, E. Plasmonics: merging photonics and electronics at nanoscale dimensions. *Science* **2006**, *311*, 189–193.
- (2) Gramotnev, D. K.; Bozhevolnyi, S. I. Plasmonics beyond the diffraction limit. *Nat. Photonics* **2010**, *4*, 83–91.
- (3) Barnes, W. L.; Dereux, A.; Ebbesen, T. W. Surface plasmon subwavelength optics. *Nature* **2003**, *424*, 824–830.
- (4) Schuller, J. A.; Barnard, E. S.; Cai, W.; Jun, Y. C.; White, J. S.; Brongersma, M. L. Plasmonics for extreme light concentration and manipulation. *Nat. Mater.* **2010**, *9*, 193–204.
- (5) Ditlbacher, H.; Krenn, J. R.; Schider, G.; Leitner, A.; Aussenegg, F. R. Two-dimensional optics with surface plasmon polaritons. *Appl. Phys. Lett.* **2002**, *81*, 1762–1764.
- (6) Radko, I. P.; Volkov, V. S.; Beermann, J.; Evlyukhin, A. B.; Søndergaard, T.; Boltasseva, A.; Bozhevolnyi, S. I. Plasmonic metasurfaces for waveguiding and field enhancement. *Laser Photonics Rev.* **2009**, *3*, 575–590.
- (7) Yin, L.; Vlasko-Vlasov, V. K.; Pearson, J.; Hiller, J. M.; Hua, J.; Welp, U.; Brown, D. E.; Kimball, C. W. Subwavelength focusing and guiding of surface plasmons. *Nano Lett.* **2005**, *5*, 1399–1402.
- (8) Liu, Z.; Steele, J. M.; Stritcuravanich, W.; Pikus, Y.; Sun, C.; Zhang, X. Focusing surface plasmons with a plasmonic lens. *Nano Lett.* **2005**, *5*, 1726–1729.
- (9) Feng, L.; Tetz, K. A.; Slutsky, B.; Lomakin, V.; Fainman, Y. Fourier plasmonics: Diffractive focusing of in-plane surface plasmon polariton waves. *Appl. Phys. Lett.* **2007**, *91*, 081101.
- (10) Bozhevolnyi, S. I.; Erland, J.; Leosson, K.; Skovgaard, P. M. W.; Hvam, J. M. Waveguiding in surface plasmon polariton band gap structures. *Phys. Rev. Lett.* **2001**, *86*, 3008–3011.
- (11) Bozhevolnyi, S. I.; Volkov, V. S.; Devaux, E.; Laluet, J. Y.; Ebbesen, T. W. Channel plasmon subwavelength waveguide components including interferometers and ring resonators. *Nature* **2006**, *440*, 508–511.
- (12) González, M. U.; Weeber, J.-C.; Baudrion, A.-L.; Dereux, A.; Stepanov, A. L.; Krenn, J. R.; Devaux, E.; Ebbesen, T. W. Design, near-field characterization, and modeling of 45° surface-plasmon Bragg mirrors. *Phys. Rev. B* **2006**, *73*, 155416.

(13) Drezet, A.; Koller, D.; Hohenau, A.; Leitner, A.; Aussenegg, F. R.; Krenn, J. R. Plasmonic crystal demultiplexer and multiports. *Nano Lett.* **2007**, *7*, 1697–1700.

(14) Zhao, C.; Zhang, J. Binary Plasmonics: launching surface Plasmon polariton to a desired pattern. *Opt. Lett.* **2009**, *34*, 2417–2419.

(15) Zhao, C.; Zhang, J. Plasmonic demultiplexer and guiding. *ACS Nano* **2010**, *4*, 6433–6438.

(16) Tanemura, T.; Balam, K. C.; Ly-Gagnon, D.; Wahl, P.; White, J. S.; Brongersma, M. L.; Miller, D. A. B. Multiple-wavelength focusing of surface plasmons with a nonperiodic nanoslit coupler. *Nano Lett.* **2011**, *11*, 2693–2698.

(17) Li, L.; Li, T.; Wang, S. M.; Zhang, C.; Zhu, S. N. Plasmonic Airy beam generated by in-plane diffraction. *Phys. Rev. Lett.* **2011**, *107*, 126804.

(18) Drezet, A.; Hohenau, A.; Koller, D.; Stepanov, A. L.; Ditlbacher, H.; Steinberger, B.; Aussenegg, F. R.; Leitner, A.; Krenn, J. R. Leakage radiation microscopy of surface Plasmon polaritons. *Mater. Sci. Eng., B* **2008**, *149*, 220–229.

(19) Drezet, A.; Hohenau, A.; Stepanov, A. L.; Ditlbacher, H.; Steinberger, B.; Galler, N.; Aussenegg, F. R.; Leitner, A.; Krenn, J. R. How to erase surface plasmon fringes. *Appl. Phys. Lett.* **2006**, *89*, 091117.

(20) Chang, S.-H.; Gray, S. K.; Schatz, G. C. Surface plasmon generation and light transmission by isolated nanoholes and arrays of nanoholes in thin metal films. *Opt. Express* **2005**, *13*, 3150–3165.